

Multipartite entanglement in the quantum tetrahedron

Robert Amelung* and Hanno Sahlmann†

*Institute for Quantum Gravity (IQG), Department of Physics,
Friedrich-Alexander-Universität Erlangen-Nürnberg (FAU),
Staudtstr. 7, 91058 Erlangen, Germany*

(Dated: January 22, 2026)

The space of $SU(2)$ -invariant four-valent tensors $\text{Inv}(j_1, j_2, j_3, j_4)$, also known as intertwiners, can be understood as the quantum states of a tetrahedron in Euclidean space with fixed areas. In loop quantum gravity, they are states of the smallest "atom of space" with non-zero volume. At the same time they correspond to four-party tensor product states invariant under global rotations. We consider the multipartite entanglement of states in $\text{Inv}(j_1, j_2, j_3, j_4)$ using the recently proposed entropic fill.

Numerically evaluating entropic fill in the case of equal spins between $1/2$ and 11 , we find that the distributions of entanglement are very different for intertwiners as compared to generic tensors, and for coherent intertwiners as compared to generic ones. The peak in the distribution seems to be at the highest entanglement for generic intertwiners and at the lowest for generic tensors, but in terms of average entanglement, the roles are switched: average entanglement is highest in arbitrary tensors and lower in intertwiners, at least in the regime of large j . We also find that entanglement depends on the geometric data of coherent intertwiners in a complicated way.

I. INTRODUCTION

Relations between entanglement and space-time geometry have been observed, investigated and even postulated in many contexts. A prime example is black hole entropy, which is associated with the geometric quantity (area) but may be understood as entanglement entropy between the outside and the inside of the black hole [1–3]. More generally, relations between entanglement and geometry have been investigated in quantum field theory, see for example [4]. In quantum gravity, entanglement is conjectured to play an important role [5]. In loop quantum gravity, various aspects of the interplay of geometry and entanglement have been investigated, see for example [6–11]. It has even been proposed that geometry itself is a form of entanglement [12].

In the present work, we are considering a very simple geometric system, the quantum tetrahedron [13, 14], and study the entanglement of its states. The smallest "atom of space" in loop quantum gravity [15–18] can be understood as a quantum tetrahedron, but the system can also be defined and studied independently. Its state space is a subspace of the space of four qudits,

$$\text{Inv}(j_1, j_2, j_3, j_4) \subset \mathbb{C}^{d_{j_1}} \otimes \mathbb{C}^{d_{j_2}} \otimes \mathbb{C}^{d_{j_3}} \otimes \mathbb{C}^{d_{j_4}}, \quad (1)$$

where $d_j = 2j + 1$ and Inv denotes the invariants under the action of $SU(2)$ in the $j_1 \otimes \dots \otimes j_4$ representation. This invariance can be understood as a closure condition for the faces of the quantum tetrahedron [17].

The geometric properties of the tetrahedron correspond to operators on this space [17, 19–21]. Since various geometric operators do not commute with each other,

the geometries have fluctuations and generically behave quantum mechanically. There are, however, special semi-classical states that are thought to describe the geometry of a classical tetrahedron geometry in an optimal way: the coherent intertwiners [22, 23].

Since this is a multiparty system, entanglement can be considered in various ways. Of particular interest is to quantify the genuine multipartite entanglement (GME), i.e., entanglement that goes beyond the bipartite entanglement between pairs of spins. In the present work we will use an intriguing measure of GME for a four-party system: the entropic fill [24]. The entropic fill is a function of the volume of a tetrahedron, suitably normalized, the geometry of which is fixed by entanglement entropy of various subsystems.

Entanglement of states of the quantum tetrahedron has been studied before. For example, the question was posed (and answered in the negative) whether there are intertwiners of valence four and higher that are absolutely maximally entangled [25–27]. While the present work was underway, the interesting publication [28] appeared. The authors investigate four-valent intertwiners systematically regarding their two-to-two entanglement: It is studied analytically, determined numerically for the group averaging of various tensors and several coherent tensors.

The present work extends the consideration of [28] in various ways. The aim is to consider and compare distributions of entropic fill in several ensembles of states, and in relation to the quantum geometry embodied in the states. To characterize and compare the entropic fill, we show and discuss the results of three different numerical approaches:

- Uniform random sampling of the various ensembles of four-party states with local dimension $2j + 1$.
- Visualization of entropic fill on the full configura-

* robert.amelung@fau.de

† hanno.sahlmann@fau.de

tion space of coherent intertwiners for classical geometric data corresponding to a tetrahedron.

- Two particular investigations of coherent intertwiners for classical geometric data not satisfying the closure condition.

Using these approaches, we study the distribution of entropic fill in various ensembles, and for various local dimensions. In particular, we determine average entropic fill in the various cases. We also investigate entropic fill as a function of the tetrahedral geometry for coherent intertwiners, and as a function of the failure to satisfy the closure condition for coherent intertwiners with non-geometric labels.

In section II we briefly introduce the quantum tetrahedron, coherent intertwiners and the entropic fill. Section III contains the results of the investigation.

In the following, we work in units in which

$$8\pi\beta\hbar G \equiv 8\pi\beta\ell_P^2 = 1, \quad (2)$$

where G is Newton's constant, β is the Barbero-Imirzi parameter of loop quantum gravity [15, 16], and ℓ_P is the Planck length.

II. FOUR-VALENT INTERTWINERS AND ENTROPIC FILL

Intertwiners – The results of the present work concern entanglement in intertwiner states, also known as invariant tensors, or equivariant maps. They are important in the recoupling theory of quantum mechanical spin. In loop quantum gravity, they are an important ingredient in constructing gauge-invariant states. Intertwiners can be understood as a linear subspace of multipartite spin states with a special "invariance" property. This property demands that the intertwiner be unchanged under simultaneous $SU(2)$ rotations of all spins. Letting j_1, \dots, j_N be the spin quantum numbers for the N parties, the invariance of intertwiner I can be expressed as

$$(D^{(j_1)}(g) \otimes \dots \otimes D^{(j_N)}(g)) I = I \quad (3)$$

for all $g \in SU(2)$, where $D^{(j)}$ is the d_j -dimensional irreducible representation of $SU(2)$. Therefore, such states are also equivalently described as having a total vanishing spin. Thus, they only exist if the N spins can combine to a total spin zero according to quantum mechanical addition of angular momenta.

For two and three parties, the invariant subspace is at most one-dimensional. Starting from four parties, however, it has several dimensions in general. In the case of equal spins $j_1 = j_2 = j_3 = j_4 =: j$, the invariant subspace is d_j -dimensional, just as every individual spin subsystem.

In loop quantum gravity, intertwiners can be thought of as quantum states of 'grains' or 'atoms' of quantized

spatial geometry. While classical geometric intuition will generally fail, one possibility is to view n -valent intertwiners as quantum states of polyhedra embedded in flat space. In particular, the four-valent intertwiners can be thought of as states of a tetrahedron. To be more precise, denote by A_i the area of the i th face of a polyhedron, and by \vec{n}_i its normal, consideration of geometric operators in quantum gravity suggests to relate

$$\sqrt{\vec{J}_i^2} \longleftrightarrow A_i, \quad \frac{\vec{J}_i}{\sqrt{\vec{J}_i^2}} \longleftrightarrow \vec{n}_i, \quad (4)$$

where \vec{J}_i denotes the i th spin operator, i.e. the generator of $D^{(j_i)}$ from Eq. (3). The invariance condition (3) therefore corresponds to the closure of the polyhedron via one of the Minkowski theorems on polyhedra [17]

$$\sum_i A_i \vec{n}_i = 0. \quad (5)$$

In this picture, the intertwiners of irreducible representations are eigenstates of areas of the polyhedron, $A_i = \sqrt{j_i(j_i + 1)}$, but not of its entire shape. Angles between surface normals in particular do not all commute with each other and are therefore not simultaneously diagonalizable. This is one motivation for the introduction of intertwiner states that describe a classical polyhedron geometry in the sense of distributing the fluctuations evenly among the degrees of freedom, which we describe in the following.

Coherent intertwiners – Semi-classical states of quantum geometry are *coherent intertwiners*. They can be understood as the projections of coherent spin state products onto the invariant subspace [22]. For a unit vector

$$\vec{n} = (\sin \theta \cos \varphi, \sin \theta \sin \varphi, \cos \theta), \quad (6)$$

the corresponding coherent spin state is an $SU(2)$ -rotated version

$$\begin{aligned} |j, \vec{n}\rangle &:= D^{(j)}(g(\vec{n})) |j, j\rangle, \\ g(\vec{n}) &:= \exp(\theta \vec{m} \cdot \vec{\tau}), \\ \vec{m} &:= (-\sin \varphi, \cos \varphi, 0) \end{aligned} \quad (7)$$

of the maximal spin state $|j, j\rangle$, where $\vec{\tau}$ are the standard anti-Hermitian generators of $SU(2)$. Its components in the non-rotated spin basis can be expressed as [22]

$$\begin{aligned} \langle j, m | j, \vec{n} \rangle &= \sqrt{\frac{(2j)!}{(j-m)!(j+m)!}} \frac{\xi^{j-m}}{(1+|\xi|^2)^j}, \\ \xi &:= \exp(-i\varphi) \tan \frac{\theta}{2}. \end{aligned} \quad (8)$$

A coherent intertwiner $I_C \in \text{Inv}(j_1, j_2, j_3, j_4)$ corresponding to four unit vectors \vec{n}_i is defined as the $SU(2)$ -average

$$I_C(\vec{n}_1, \vec{n}_2, \vec{n}_3, \vec{n}_4) := \int_{SU(2)} dg \bigotimes_{i=1}^4 D^{(j_i)}(g) |j_i, \vec{n}_i\rangle \quad (9)$$

of a product of four coherent spin states, which amounts to a projection to the invariant subspace. Such intertwiners are invariant (up to a phase factor) under a simultaneous $SO(3)$ rotation of all four vectors \vec{n}_i . When they fulfill the *closure condition*

$$j_1\vec{n}_1 + j_2\vec{n}_2 + j_3\vec{n}_3 + j_4\vec{n}_4 = \vec{0}, \quad (10)$$

they can be understood as the outward (normalized) surface normals of the intertwiner's tetrahedral picture.

Entropic fill – The recently proposed *entropic fill* [24] permits quantitative comparisons of genuine multipartite entanglement in four-qubit systems. Generalizing their triangle measure of tripartite entanglement [29], the authors introduced an *entropic tetrahedron* for four-qubit states. Its construction relies on the property that the inscribed sphere of a tetrahedron defines 12 triangular regions on its faces with areas σ_{ij} ; pairs sharing an edge have the same area (see Fig. 1). The six-parameter set $\{\sigma_{12}, \sigma_{13}, \sigma_{14}, \sigma_{23}, \sigma_{24}, \sigma_{34}\}$ fixes the volume V by

$$\begin{aligned} V &= \frac{\sqrt{2}}{3} \sqrt{S} (A_0 A_1 A_2 A_3)^{1/4}, \\ S &:= 2 \cdot (\sigma_{12} + \sigma_{13} + \sigma_{14} + \sigma_{23} + \sigma_{24} + \sigma_{34}), \\ A_0 &:= +\sqrt{\sigma_{12}\sigma_{34}} + \sqrt{\sigma_{13}\sigma_{24}} + \sqrt{\sigma_{14}\sigma_{23}}, \\ A_1 &:= -\sqrt{\sigma_{12}\sigma_{34}} + \sqrt{\sigma_{13}\sigma_{24}} + \sqrt{\sigma_{14}\sigma_{23}}, \\ A_2 &:= +\sqrt{\sigma_{12}\sigma_{34}} - \sqrt{\sigma_{13}\sigma_{24}} + \sqrt{\sigma_{14}\sigma_{23}}, \\ A_3 &:= +\sqrt{\sigma_{12}\sigma_{34}} + \sqrt{\sigma_{13}\sigma_{24}} - \sqrt{\sigma_{14}\sigma_{23}}. \end{aligned} \quad (11)$$

For the entropic fill, the parameters are obtained from the bipartite entanglement entropies of the seven possible bipartitions of the four-qubit system: four *one-to-other* entropies $E_{i(jkl)}$ and three *two-to-two* entropies $E_{(ij)(kl)}$, defined using the base-two logarithm. They define the σ_{ij} by the following set of equations:

$$\sigma_{ij} + \sigma_{ik} + \sigma_{il} = E_{i(jkl)}, \quad (12)$$

$$-\sqrt{\sigma_{ij}\sigma_{kl}} + \sqrt{\sigma_{ik}\sigma_{jl}} + \sqrt{\sigma_{il}\sigma_{jk}} = \lambda E_{(ij)(kl)}, \quad (13)$$

for all index permutations (seven non-equivalent equations), where λ is an additional non-physical variable determined from the entropies. These equations ensure that the one-to-other entropies are the areas of the faces of the entropic tetrahedron – permitted by qubit entanglement polygon inequalities [30] – while the two-to-two entropies determine the overall shape given these constraints. The authors provided strong evidence for the existence of non-negative solutions for all four-qubit states. The entropic fill F_4 is defined as

$$F_4 = (3^{7/6}/2) V^{2/3}, \quad (14)$$

where the pre-factor is added for normalization $0 \leq F_4 \leq 1$, while the exponent permits additivity of the resulting measure.

As noted in [24], entropic fill may be suitably generalized to four-*qudit* systems, since polygon inequalities

hold in that case as well [31]. Because the maximal value of bipartite entropies depends on the local dimensions, we chose to normalize all entropies – so that $0 \leq E \leq 1$ – before plugging into the equations. Note that since V is homogeneous in σ_{ij} , this is equivalent to dividing by the maximal F_4 at the end instead. Indeed, the maximal volume is obtained when all σ_{ij} are equal to $1/3$ of the maximal one-to-other entropy (regular entropic tetrahedron).

The normalization of the two-to-two entropies is irrelevant, as it can be absorbed into λ . This means that four-qudit states need not be *perfect*, in the sense of maximal entanglement for all possible bipartitions, to exhibit maximal entropic fill. It suffices that the one-to-other entropies are maximal, while the two-to-two entropies all have the same value. Note that if one-to-other entropies are non-zero, not all two-to-two entropies can vanish simultaneously [32].

When numerically solving the defining equations in samples of considerable size, we consistently encountered final minimization costs near machine precision, suggesting that the entropic fill is indeed well-defined for four-qudit states.

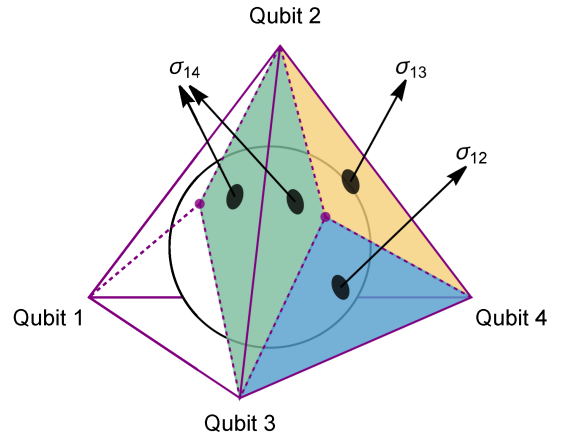


FIG. 1. The inscribed sphere touches each face at a point, defining 12 triangles on the faces. Pairs of triangles sharing an edge have the same area σ_{ij} . The vertices are numbered so that σ_{ij} is the area of each of the two triangles sharing the edge between the faces opposite vertices i and j . This figure has been re-used without modification from [24] under the license CC BY 4.0.

III. RESULTS

General properties – As can be shown using orthogonality relations of the $3j$ -symbol, the one-to-other entropies of intertwiners are always maximal [25], so the entropic tetrahedra are *equifacial* for those states; such tetrahedra are also called *disphenoids*. The two-to-two entropies of four-valent intertwiners cannot all be maximal simultaneously [25]. Nevertheless, the coherent

intertwiner corresponding to a regular tetrahedron is maximally entangled according to entropic fill. Indeed, the proper rotational symmetries of a regular tetrahedron contain, in particular, rotations cyclically permuting three of the four normal vectors. Since exchanging normal vectors correspondingly (inversely) permutes components of the tensor, its three two-to-two entropies must be identical. Note that general disphenoids only exhibit 180° rotational symmetries which translate into pairwise – not cyclic – exchanges of indices, so the entropic fill of coherent intertwiners is not maximal in general.

Sampled distributions – To compare the entropic fill among different types of four-spin states, we numerically sampled 5×10^5 randomly chosen tensors for each of four different cases at small values of j : arbitrary; invariant; coherent with and without a fulfilled closure condition. Arbitrary tensors were sampled uniformly with respect to the Fubini-Study metric from the unit sphere in $\mathbb{C}^{d_j^4}$; the components were interpreted in the standard spin product basis. Similarly, invariant tensors were sampled uniformly from the unit sphere in \mathbb{C}^{d_j} , interpreted within a specific orthonormal basis of $\text{Inv}(j^{\otimes 4})$. For the coherent intertwiners without closure, we independently chose four unit vectors in \mathbb{R}^3 , sampled uniformly from the unit sphere, and computed the corresponding tensor.

However, to generate random unit vectors which close, one must proceed differently. The space of four-tuples of unit vectors – modulo proper rotations – whose sum vanishes has two degrees of freedom [33]. As one of the two, we chose the angle $\theta \in (0, \pi)$ between \vec{n}_1 and \vec{n}_2 . Given these two vectors, the endpoints of \vec{n}_3 and \vec{n}_4 are restricted to the intersection between the unit sphere and the sphere of center $-\vec{n}_1 - \vec{n}_2$ and radius one, which is a circle. The angle $\phi \in [0, 2\pi]$ along this circle was chosen as the second parameter. The induced uniform probability distribution dictates that θ be chosen according to $\sin(\theta/2)/2$, while ϕ is selected uniformly [34]. Note that in the non-closure case, θ follows a $\sin(\theta)/2$ distribution. We thus sampled \vec{n}_1 and \vec{n}_2 accordingly, followed by determining \vec{n}_3 on the circle and choosing $\vec{n}_4 = -\sum_{i=1}^3 \vec{n}_i$. Absolute orientation of the four-tuple is irrelevant for measures of entanglement.

Note that the sampling for the ensembles of coherent intertwiners is thus uniform in their parameter space, but does not make reference to the Fubini-Study volume.

Distributions for $j \in \{0.5, 1.5, 3\}$ are shown in Fig. 2, while means are shown as a function of j in Fig. 3. The mean entanglement seems to increase fastest for arbitrary states and general intertwiners, out-performing coherent intertwiners. Within the coherent category, the closure condition leads to slightly higher entropic fill for spin values up to about $j = 7$. Moreover, coherent intertwiners – especially those with closure – exhibit narrow peaks of comparably very likely entropic fill values. Analysis of our minimization costs for the equation-solving indicates that these are not

mere numerical artifacts and instead suggest some interesting structure within the coherent intertwiner space. Arbitrary states exhibit a peak around their mean entropic fill, while general intertwiners have a clear increasing preference for near-maximal values. For coherent intertwiners, the distribution drops much slower to zero at lower entropic fill than the other two categories.

Full configuration space – We further show numerically computed entropies and entropic fill in the full (θ, ϕ) configuration space of coherent intertwiners with closure, in Fig. 4 for $j = 1/2$ and Fig. 5 for $j = 3/2$. We evaluated 300×300 regularly spaced points in the configuration space. For this, \vec{n}_1 was set to the unit vector in the y -direction, and $\vec{n}_2 = (\sin \theta, \cos \theta, 0)$. Then we chose coordinate unit vectors for the plane of the circle of possible $\vec{n}_{3,4}$ -endpoints, namely the \hat{z} unit vector together with $(\vec{n}_1 + \vec{n}_2)/||\vec{n}_1 + \vec{n}_2|| \times \hat{z}$. Then the angular parameter $\phi \in [0, 2\pi)$ for \vec{n}_3 corresponds to turning around the circle in the positive sense. Note that the endpoints of \vec{n}_3 and \vec{n}_4 are always antipodal on this circle, so E_{13} and E_{14} are equal up to a translation $\phi \rightarrow \phi + \pi$. Note also that area elements in these plots are not equally likely for a random coherent intertwiner with closure; in fact, θ near π is more likely than near zero.

For small values of θ , \vec{n}_3 and \vec{n}_4 are restricted to a small circle, explaining the entropies' and entropic fill's approximate independence of ϕ in that region. This independence even goes up to values above $\theta = \pi/2$ for E_{12} . Furthermore, the regular tetrahedron configurations ($\theta = \arccos(-1/3)$, $\phi \in \{0, \pi\}$) show as islands of maximal entropic fill. The peaks in Fig. 2 correspond to (parts of) the white stripes.

We also show the mean entropies and entropic fill of coherent intertwiners with closure as a function of θ in Fig. 6 for $j \in \{0.5, 1.5, 3\}$. For this, we sampled 500 equally spaced values of ϕ for each of 300 equally spaced values of θ . Note that since E_{13} and E_{14} are related by ϕ -translational symmetry, their means coincide. We observe dips in mean entropic fill around $\theta = \pi/2$ and near $\theta = \pi$, whose depth decreases as j increases. We observe no particular structure near the regular tetrahedral angle $\theta \approx 1.91$. The mean two-to-two entropy \bar{E}_{12} exhibits a peak near $\theta = \pi/2$, which agrees with numerical computational results in [28].

Particular configurations – As a final investigation into the entanglement of coherent intertwiners, we chose two particular *base configurations* – a regular tetrahedron, and a *tetragonal disphenoid* (isosceles faces) – and numerically computed the entropic fill as a function of the first unit vector, while the other three remained fixed. Closure is thus obtained only at one particular \vec{n}_1 . The following base configuration polar coordinates were cho-

sen for the regular tetrahedron:

$$(\varphi_1, \varphi_2, \varphi_3, \varphi_4) = \left(-\frac{\pi}{4}, -\frac{3\pi}{4}, \frac{\pi}{4}, \frac{3\pi}{4}\right),$$

$$(\cos \theta_1, \cos \theta_2, \cos \theta_3, \cos \theta_4) = \left(-\frac{1}{\sqrt{3}}, \frac{1}{\sqrt{3}}, \frac{1}{\sqrt{3}}, -\frac{1}{\sqrt{3}}\right).$$

For the tetragonal disphenoid, we set

$$(\varphi_1, \varphi_2, \varphi_3, \varphi_4) = \left(-\frac{\pi}{2}, \frac{3\pi}{4}, -\frac{\pi}{2}, \frac{\pi}{4}\right),$$

$$(\theta_1, \theta_2, \theta_3, \theta_4) = \left(\frac{\pi}{4}, \frac{\pi}{2}, \frac{3\pi}{4}, \frac{\pi}{2}\right).$$

The results are shown in Fig. 7 for $j = 1/2$, and in Fig. 8 for $j = 3/2$, where we sampled a regular grid of 300×300 pairs of $\cos \theta_1$ and φ_1 . In these plots, every area element is equally likely when choosing \vec{n}_1 uniformly on the unit sphere.

In absolute terms (left plots), we see clear relative dips in entropic fill at three distinct coordinate pairs. When plotting logarithmically (right plots), we see two peaks of near-maximal entropic fill. For the regular tetrahedron, one of them lies at the base configuration as expected, but there is a second one. For the tetragonal disphenoid, the peaks are very narrow. These examples suggest interesting entanglement structure within near-closing coherent intertwiners.

IV. DISCUSSION AND OUTLOOK

In the present work we have used entropic fill to characterize entanglement in intertwiners, i.e., tensors invariant under rotations. This continues and complements other work [25–28].

We compared entanglement distributions for several ensembles of four-valent tensors: arbitrary ones, generic invariant ones, and of coherent invariant tensors with and without closure for the classical data. While average entanglement is generally quite high and approaching its maximum for large j in all ensembles as expected, the shape of the distributions is surprisingly different in the different ensembles (Fig. 2). Mean entanglement grows at different rates in the different ensembles and seems to be highest in the ensemble of arbitrary tensors for large j (Fig. 3). Entanglement of invariant tensors peaks at the maximum possible value, whereas arbitrary tensors have a well defined peak below maximum (Fig. 2). The distribution for coherent intertwiners shows a lot of structure, for example two sharp peaks for the coherent intertwiners with closure, and one sharp peak for those without (Fig. 2). It is interesting that these two ensembles seem to behave so differently, at least for low spin.

Note that the sampling for the ensembles of coherent intertwiners is uniform in their parameter space, but does not make reference to the Fubini-Study volume. This is a natural choice, but comparison with the other ensembles is then not necessarily straightforward. It could be interesting to also implement a different sampling, perhaps

by pulling back the Fubini-Study metric to the space of coherent intertwiners.

For the coherent intertwiners we also investigated the dependence of entanglement on the classical geometry that they approximate. The resulting picture is complex (Fig. 4–6): Entanglement depends on the geometry, but we did not find an interpretation in terms of simple properties of the classical configurations such as, for example, the relative position of the surface normals. Regarding the effects of (non-)closure of the classical data, the situation is similarly intriguing. The entanglement is higher in the closed configuration than in a typical non-closed one, but the closed configuration is not always the location of the maximum entanglement (Fig. 7, 8).

We should note that, by solving Eqs. (12), (13) for a large number of intertwiners and thus associating an entropic tetrahedron in each case, we have added to the strong numerical evidence [24] that entropic fill is defined for any local dimension.

As a final point of discussion, both the quantum geometry and the entanglement measure F_4 studied in this work are related to the tetrahedron. The areas of the entropic triangle are determined by the (normalized) one-to-other von-Neumann entropies. For intertwiners it is maximal, $\log_2 d_j$ without normalization for a spin j party. The area of the geometric triangle also depends on j , albeit in a different way, $a_j \propto \sqrt{j(j+1)}$. For the rest of the degrees of freedom of a tetrahedron, the relationship is more complex and indirect, see Fig. 4, Fig. 5.

In loop quantum gravity, quantum states have geometrical meaning [15, 16]. This ties into a larger story about entanglement in quantum gravity [2–5]. Our work sheds light on just a small aspect of the correlation between geometric properties and properties of the states in terms of quantum information. As a direct continuation of the present work, it would be interesting to better understand the structures seen in the entanglement of coherent intertwiners. More generally, long-range entanglement in loop quantum gravity results from states that are not product states with respect to the intertwiners at different vertices [6–8]. It would be very interesting to understand this type of entanglement and its relation to the geometry better, in particular also for solutions to the quantum constraints, a form of Einstein’s equations in the quantum theory [15, 16].

ACKNOWLEDGMENTS

HS acknowledges the contribution from COST Action BridgeQG (CA23130), supported by COST (European Cooperation in Science and Technology).

DATA AND CODE AVAILABILITY

All code used and data created for this publication is available on GitHub [35].

[1] D. N. Page, Information in black hole radiation, *Phys. Rev. Lett.* **71**, 3743 (1993), arXiv:hep-th/9306083.

[2] L. Bombelli, R. K. Koul, J. Lee, and R. D. Sorkin, A Quantum Source of Entropy for Black Holes, *Phys. Rev. D* **34**, 373 (1986).

[3] A. Perez, Statistical and entanglement entropy for black holes in quantum geometry, *Phys. Rev. D* **90**, 084015 (2014), [Addendum: *Phys. Rev. D* 90, 089907 (2014)], arXiv:1405.7287 [gr-qc].

[4] M. Srednicki, Entropy and area, *Phys. Rev. Lett.* **71**, 666 (1993), arXiv:hep-th/9303048.

[5] E. Bianchi and R. C. Myers, On the Architecture of Spacetime Geometry, *Class. Quant. Grav.* **31**, 214002 (2014), arXiv:1212.5183 [hep-th].

[6] E. R. Livine, Intertwiner Entanglement on Spin Networks, *Phys. Rev. D* **97**, 026009 (2018), arXiv:1709.08511 [gr-qc].

[7] B. Baytaş, E. Bianchi, and N. Yokomizo, Gluing polyhedra with entanglement in loop quantum gravity, *Phys. Rev. D* **98**, 026001 (2018), arXiv:1805.05856 [gr-qc].

[8] E. Bianchi, P. Donà, and I. Vilensky, Entanglement entropy of Bell-network states in loop quantum gravity: Analytical and numerical results, *Phys. Rev. D* **99**, 086013 (2019), arXiv:1812.10996 [gr-qc].

[9] D. Grüber, H. Sahlmann, and T. Zilker, Geometry and entanglement entropy of surfaces in loop quantum gravity, *Phys. Rev. D* **98**, 066009 (2018), arXiv:1806.05937 [gr-qc].

[10] E. Bianchi and E. R. Livine, Loop quantum gravity and quantum information, in *Handbook of Quantum Gravity*, edited by C. Bambi, L. Modesto, and I. Shapiro (Springer Nature Singapore, Singapore, 2023) pp. 1–29.

[11] H. Sahlmann and M. Zeiß, Bell states for fermions in loop quantum gravity, arXiv:2508.04704 [gr-qc] (2025).

[12] J. Maldacena and L. Susskind, Cool horizons for entangled black holes, *Fortsch. Phys.* **61**, 781 (2013), arXiv:1306.0533 [hep-th].

[13] A. Barbieri, Quantum tetrahedra and simplicial spin networks, *Nucl. Phys. B* **518**, 714 (1998), arXiv:gr-qc/9707010.

[14] J. C. Baez and J. W. Barrett, The Quantum tetrahedron in three-dimensions and four-dimensions, *Adv. Theor. Math. Phys.* **3**, 815 (1999), arXiv:gr-qc/9903060.

[15] T. Thiemann, Introduction to Modern Canonical Quantum General Relativity, arXiv:gr-qc/0110034 (2001).

[16] A. Ashtekar and J. Lewandowski, Background independent quantum gravity: A Status report, *Class. Quant. Grav.* **21**, R53 (2004), arXiv:gr-qc/0404018.

[17] E. Bianchi, P. Doná, and S. Speziale, Polyhedra in loop quantum gravity, *Phys. Rev. D* **83**, 044035 (2011).

[18] H. M. Haggard, J. Lewandowski, and H. Sahlmann, Emergence of Riemannian Quantum Geometry, arXiv:2302.02840 [gr-qc] (2023).

[19] A. Ashtekar and J. Lewandowski, Quantum theory of geometry. 1: Area operators, *Class. Quant. Grav.* **14**, A55 (1997), arXiv:gr-qc/9602046.

[20] A. Ashtekar and J. Lewandowski, Quantum theory of geometry. 2. Volume operators, *Adv. Theor. Math. Phys.* **1**, 388 (1998), arXiv:gr-qc/9711031.

[21] S. A. Major, Operators for quantized directions, *Class. Quant. Grav.* **16**, 3859 (1999), arXiv:gr-qc/9905019.

[22] E. R. Livine and S. Speziale, New spinfoam vertex for quantum gravity, *Phys. Rev. D* **76**, 084028 (2007).

[23] E. Alesci, J. Lewandowski, and I. Mäkinen, Coherent 3j-symbol representation for the loop quantum gravity intertwiner space, *Phys. Rev. D* **94**, 084028 (2016), arXiv:1606.06561 [gr-qc].

[24] S. Xie, D. Younis, Y. Mei, and J. H. Eberly, Multipartite entanglement: A journey through geometry, *Entropy* **26**, 10.3390/e26030217 (2024).

[25] Y. Li, M. Han, M. Grassl, and B. Zeng, Invariant Perfect Tensors, *New J. Phys.* **19**, 063029 (2017), arXiv:1612.04504 [quant-ph].

[26] R. Mansuroglu and H. Sahlmann, No invariant perfect qubit codes, *JHEP* **02**, 062, arXiv:2210.02483 [quant-ph].

[27] F. Otto, R. Mansuroglu, N. Schuch, O. Gühne, and H. Sahlmann, Hyperinvariant Spin Network States – An AdS/CFT Model from First Principles, arXiv:2510.06602 [quant-ph] (2025).

[28] G. Long, Q. Chen, and J. Yang, Entanglement entropy of coherent intertwiner in loop quantum gravity, *Phys. Rev. D* **110**, 064017 (2024).

[29] S. Xie and J. H. Eberly, Triangle measure of tripartite entanglement, *Phys. Rev. Lett.* **127**, 040403 (2021).

[30] X.-F. Qian, M. A. Alonso, and J. H. Eberly, Entanglement polygon inequality in qubit systems, *New Journal of Physics* **20**, 063012 (2018).

[31] X. Yang, Y.-H. Yang, and M.-X. Luo, Entanglement polygon inequality in qudit systems, *Phys. Rev. A* **105**, 062402 (2022).

[32] M. Ruskai, Inequalities for quantum entropy: A review with conditions for equality, *Journal of Mathematical Physics* **43** (2002).

[33] M. Kapovich and J. J. Millson, The symplectic geometry of polygons in Euclidean space, *Journal of Differential Geometry* **44**, 479 (1996).

[34] J. Cantarella and C. Shonkwiler, The symplectic geometry of closed equilateral random walks in 3-space, *The Annals of Applied Probability* **26**, 549 (2016).

[35] R. Amelung and H. Sahlmann, Code and data for the intertwiner entropic fill project, Available at: <https://github.com/R-Amelung/IntertwinerEntFill.git> (2026).

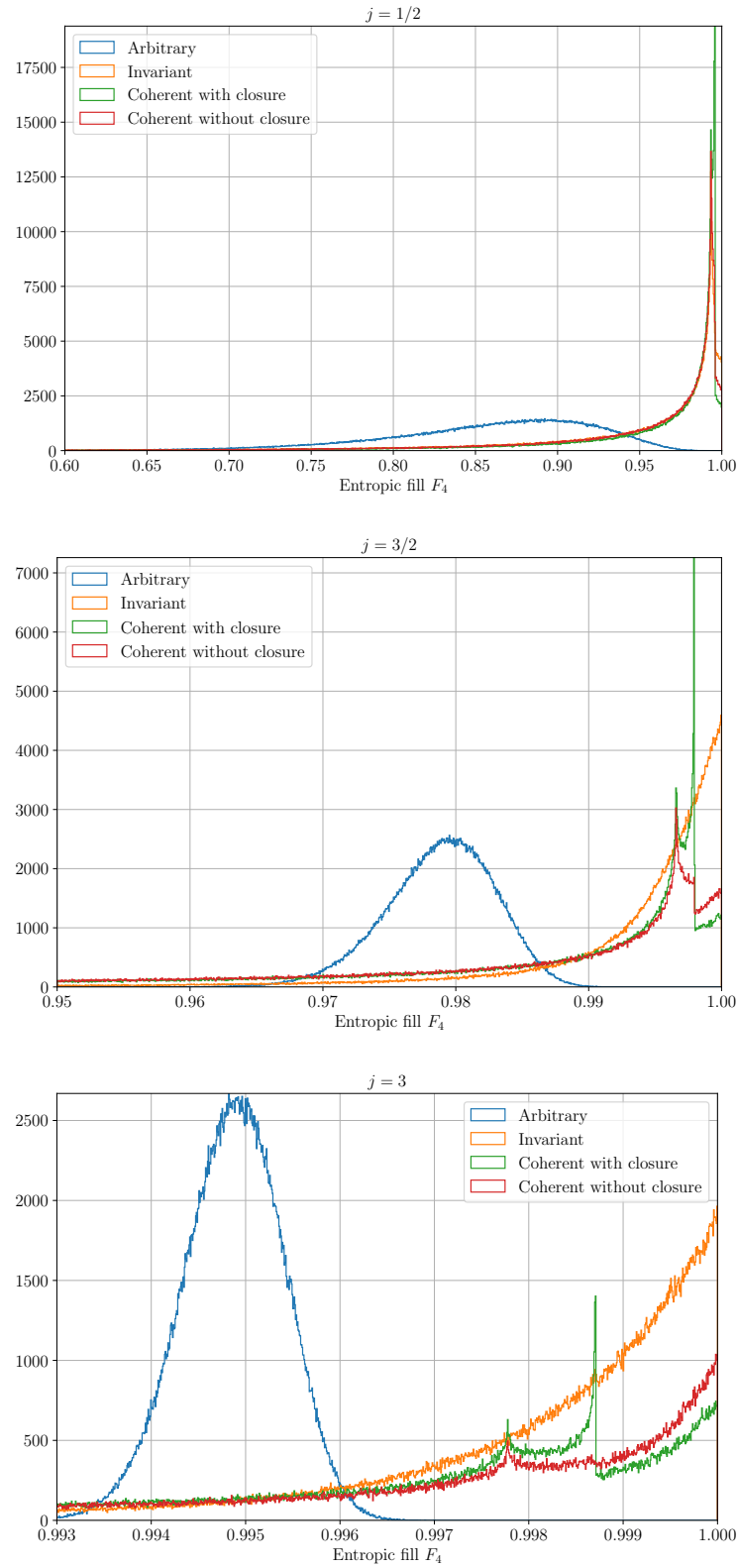


FIG. 2. Sampled distributions of entropic fill for arbitrary states, invariant intertwiners, and coherent intertwiners with and without closure (5×10^5 for each). We show 1000 bins in the interesting parts near maximal entropic fill (note the bounds on the x -axis for each plot) for $j \in \{0.5, 1.5, 3\}$. Below these regions, the bins have comparably neglectable counts. Average entropic fill of arbitrary states and general intertwiners increases more rapidly with increasing j than both types of coherent intertwiners, explaining the apparent change in relative counts from one plot to the next.

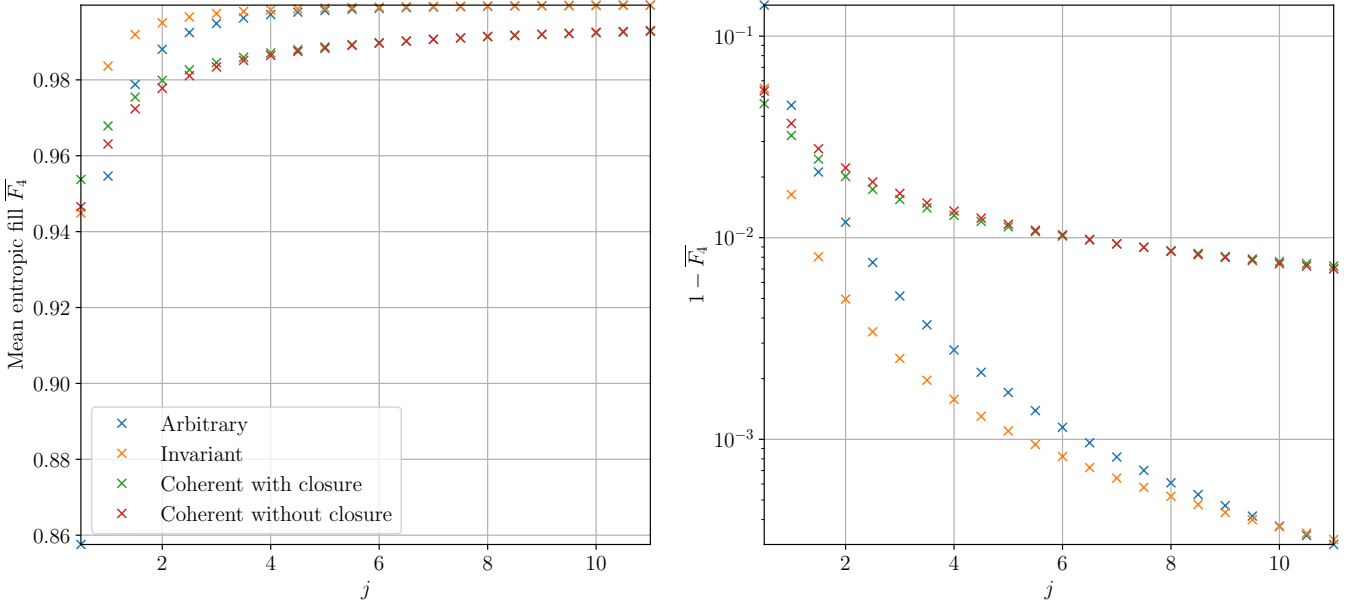


FIG. 3. Numerically computed means of entropic fill for arbitrary states, invariant intertwiners, and coherent intertwiners with and without closure (sample size 5×10^5 for each), for j ranging from $1/2$ to 11 . We show absolute entropic fill on the left, and the distance from maximal entropic fill on the right (logarithmic scale). All visible differences are well within statistical certainty, the standard errors of the means being at least an order of magnitude smaller at this sample size (except for the two coherent intertwiner categories between $j = 6.5$ and $j = 7.5$ and the two other categories near $j = 10$). The mean entanglement increases fastest for arbitrary states and general intertwiners, out-performing coherent intertwiners. Within the coherent category, the closure condition leads to slightly higher entropic fill for spin values up to about $j = 7$.

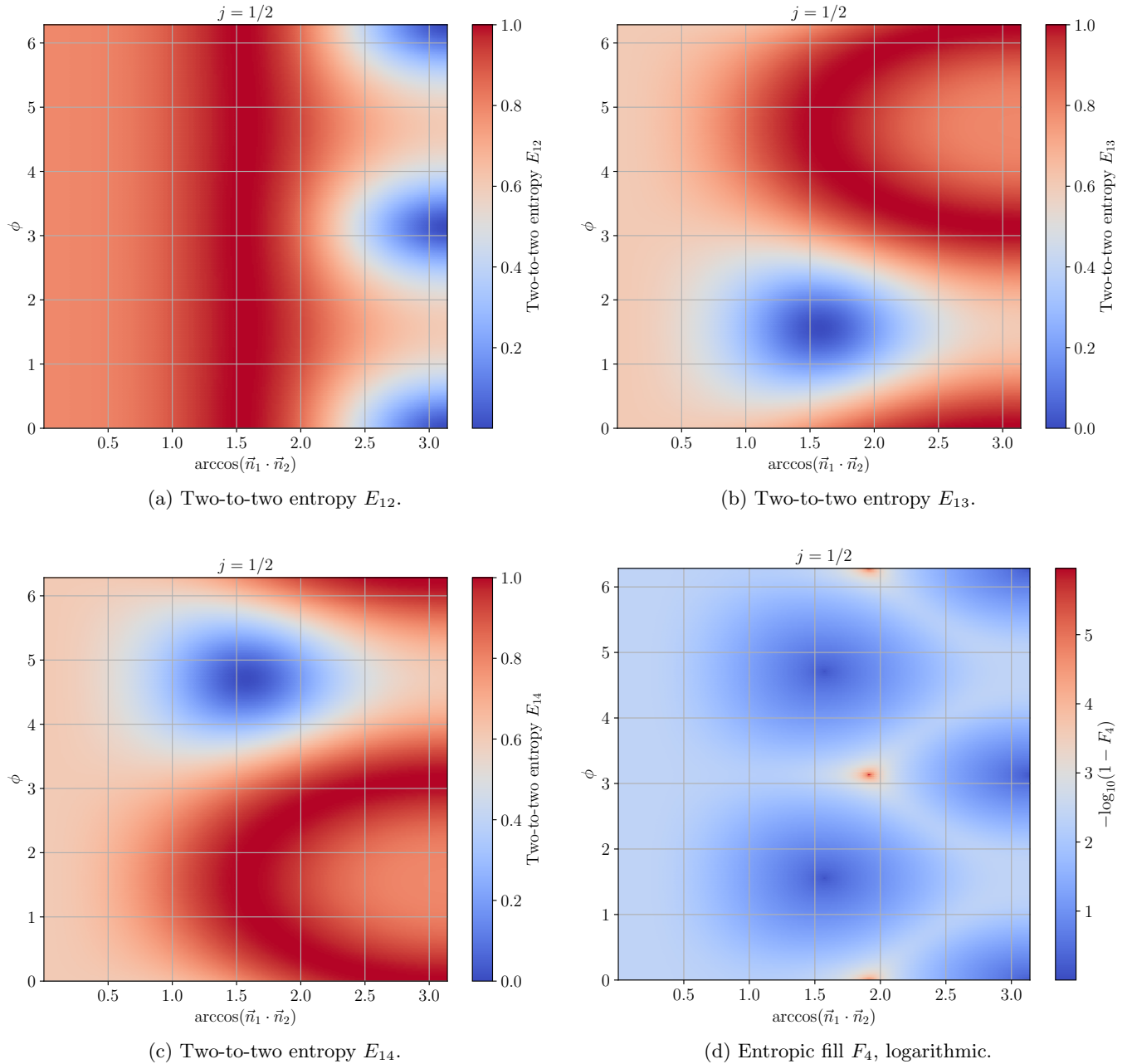
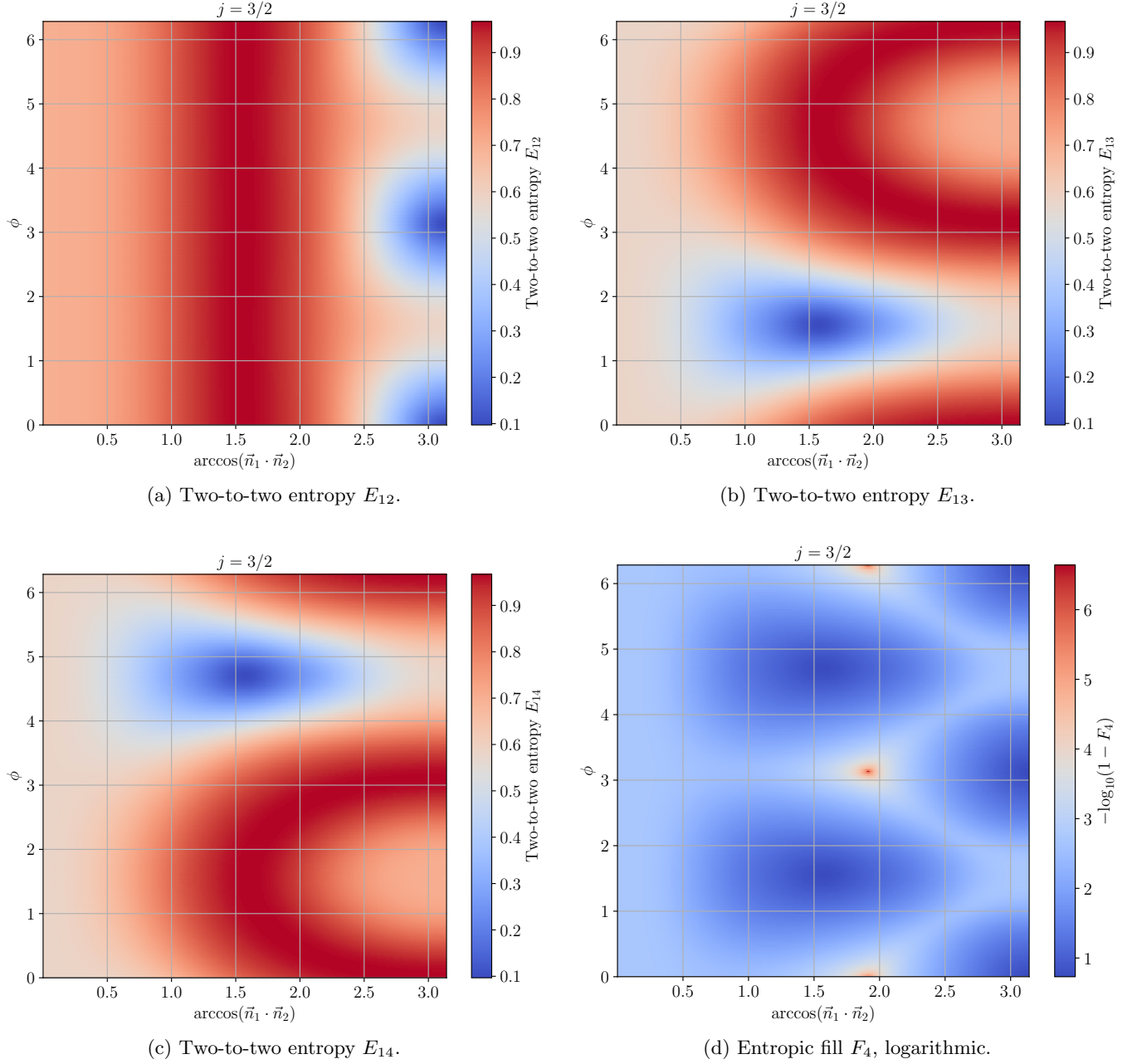


FIG. 4. Numerically computed (300×300) two-to-two entropies and (logarithmic inverse distance from maximal) entropic fill on the configuration space of coherent intertwiners with closure for $j = 1/2$; the x -axis encodes the angle θ between \vec{n}_1 and \vec{n}_2 , while the y -axis represents the angle on the circle of possible endpoints for \vec{n}_3 given \vec{n}_1 and \vec{n}_2 . The regular tetrahedron configurations appear as spots of maximal entropic fill. Note that not every area element in these plots is equally likely for a random coherent intertwiner with closure; in fact, θ near π is more likely than near zero.

FIG. 5. Idem Fig. 4 with $j = 3/2$.

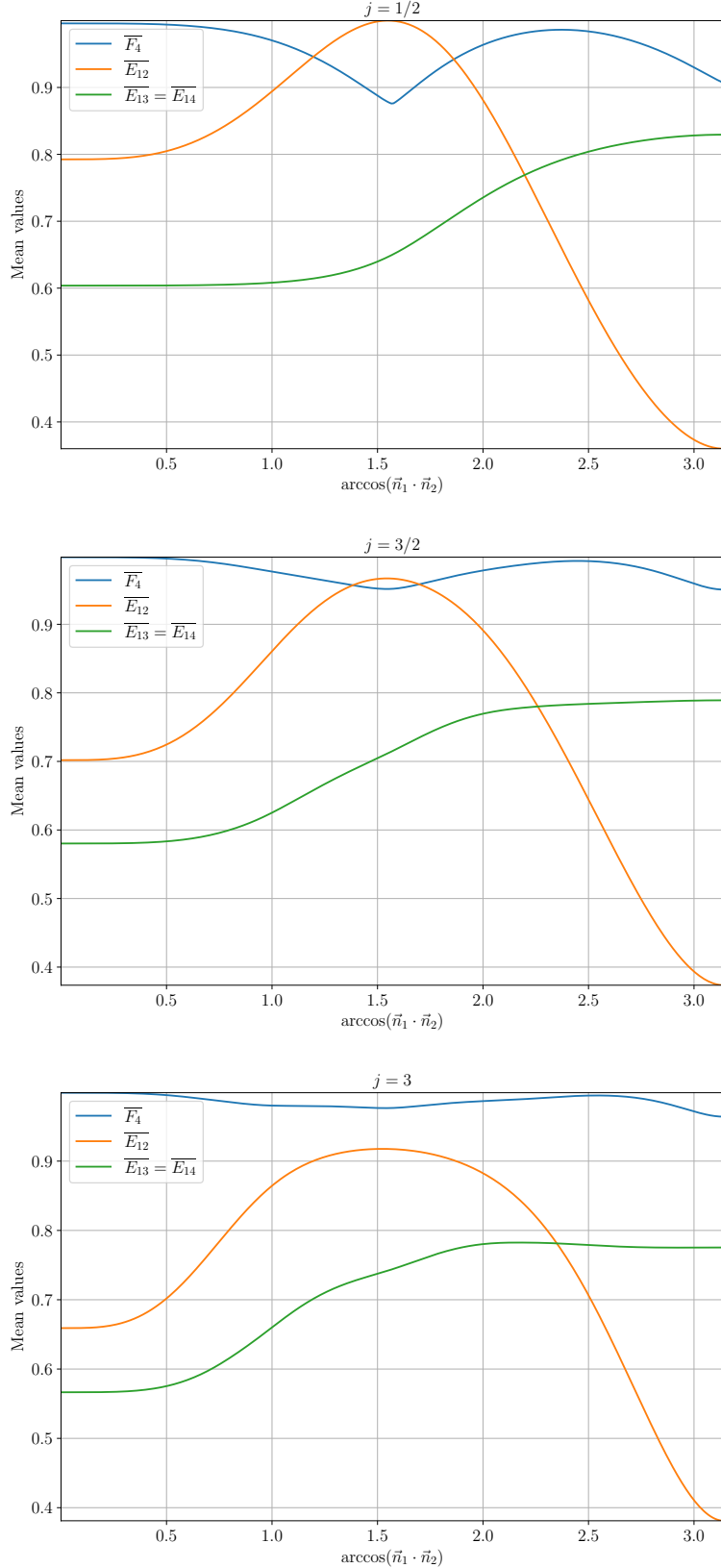


FIG. 6. Numerically computed mean two-two-to entropies and entropic fill of coherent intertwiners with closure, as a function of the angle θ between \vec{n}_1 and \vec{n}_2 , for $j \in \{0.5, 1.5, 3\}$. We sampled 500 equally spaced values of ϕ for each of 300 equally spaced values of θ .

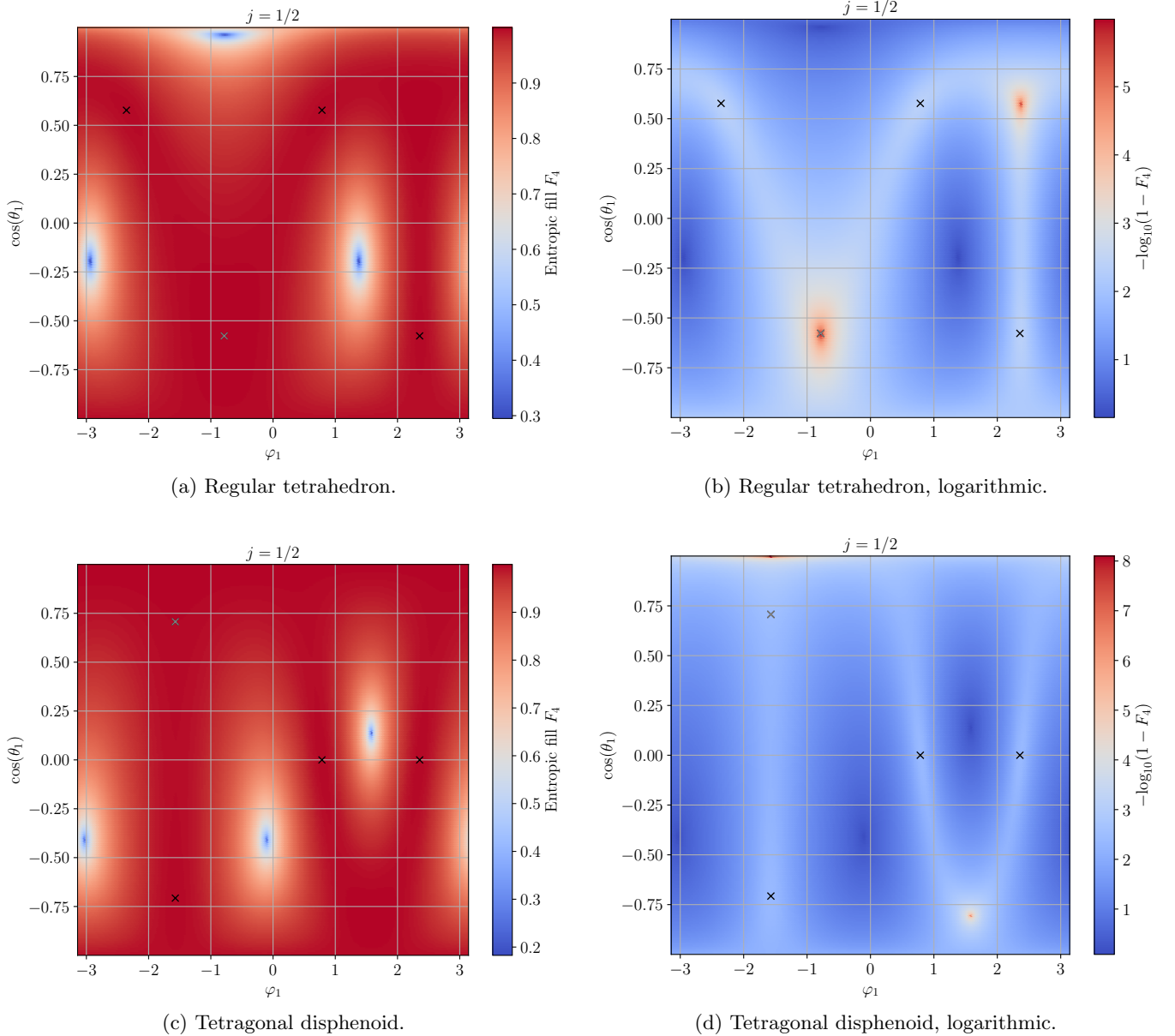
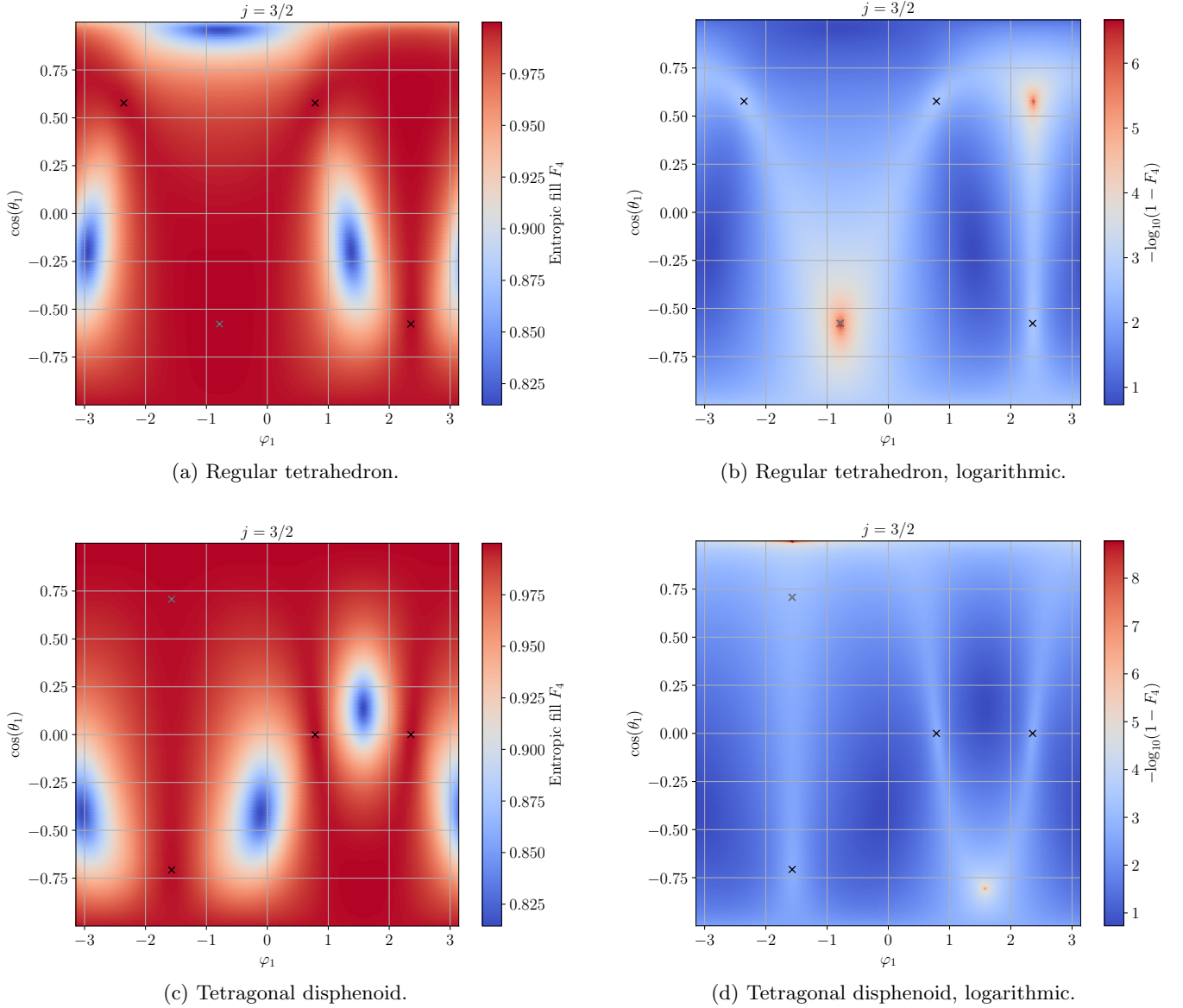


FIG. 7. Numerically computed entropic fill for the regular tetrahedron and the tetragonal disphenoid base configurations for $j = 1/2$, as a function of the azimuthal angle φ_1 and the cosine of the polar angle $\cos(\theta_1)$ of \vec{n}_1 . Black crosses denote the coordinates of the other three normal vectors; a gray cross is placed at the coordinates of the closure condition for \vec{n}_1 . We show absolute entropic fill on the left, and logarithmic inverse distance from maximal entropic fill on the right. In these plots, every area element is equally likely.

FIG. 8. Idem Fig. 7 with $j = 3/2$.